Pattern Recognition Letters 47 (2014) 164–171

Contents lists available at ScienceDirect

Pattern Recognition Letters

journal homepage: www.elsevier.com/locate/patrec

Automatic retinal vessel extraction based on directional mathematical morphology and fuzzy classification ☆

Eysteinn Már Sigurðsson [a], Silvia Valero [b], Jón Atli Benediktsson [a,*], Jocelyn Chanussot [a,c], Hugues Talbot [d], Einar Stefánsson [e]

[a] Faculty of Electrical and Computer Engineering, University of Iceland, Reykjavik, Iceland
[b] CESBIO Laboratory, 18 Avenue Edouard Belin bpi 2801, 31401 Toulouse cedex 9, France
[c] GIPSA-Lab, Grenoble Institute of Technology, Grenoble, France
[d] IGM-A2SI-ESIEE, BP 99-2 Bd Blaise-Pascal, 93162 Noisy-le-Grand, France
[e] Department of Ophthalmology, Faculty of Medicine, University of Iceland, Reykjavik, Iceland

ARTICLE INFO

Article history:
Available online 25 March 2014

Keywords:
Fundus image
Mathematical morphology
Path openings
Image fusion
Fuzzy sets

ABSTRACT

The problem of detecting blood vessels in retinal color fundus images is addressed. An unsupervised method based on the extraction of two vessel features vectors in order to detect the pixels belonging to the vessel tree is presented. The proposed vessel features rely on the contrast of vessels and their linear connectivity. The extraction of these features is performed by using advanced morphological directional filter called path openings. The resulting features are used to carry out a data fusion task based on fuzzy set theory. As a result, pixel classification can easily be performed to construct a vessel map. Experimental results using real data have demonstrated the ability of the proposed method to successfully extract a good quality vessel tree. The obtained results are compared with results obtained by classical vessel extraction techniques.

1. Introduction

The detection of vessels from medical imaging plays an important role in a wide range of clinical research. The assessment of retinal metabolism and structure can allow evaluation of the pathophysiology of common eye diseases such as retinal vascular occlusions [8], diabetic retinopathy [9], age-related macular degeneration, glaucoma [19] and to study chronic systemic hypoxemia [30]. To be able to characterize such abnormalities, the geometric characterization of the blood vessels has a considerable interest. Furthermore, the construction of a well-defined vessel segmentation enables to quantify the disease severity or to evaluate the progress of one therapy. In practice, manual segmentation of vessels still remains widely used. The human intervention is extremely time consuming and it implies a large variability caused by some factors such as fatigue effects. Hence, a reliable automatic vessel segmentation method is necessary. In the literature, many works have been published about the detection of vessels in medical images.

A significant number of the previously published techniques are based on matched filters. For instance, in [2], 12 different matched filter templates are constructed to detect piecewise linear segments of blood vessels in all possible directions. In this context, in [11] the method is improved by probing the area of the matched filter response image while iterating the threshold and [4] uses an amplitude modified Gaussian filter to account for diameter measurement of blood vessels.

Supervised approaches [24] where multilayer perceptron neural network is used with inputs derived from principal component analysis of pixel values of RGB images and the image edges. In [28] classification is based on the eigen-decomposition of the Hessian for each pixel in the image. [23] use SVM to classify pixel based on three features that are extracted using two orthogonal rotated linear structuring elements of different lengths and the pixel intensity.

Another important family of vessel detection techniques is based on the well-known mathematical morphology theory [35,33,7,34,21,17]. These techniques use morphology in order to detect the linear structures forming the vessel tree. The operators strongly depend on the shape of the chosen structuring element. For this reason, classical morphological filters are not flexible

☆ This paper has been recommended for acceptance by Cris L. Luengo Hendriks.

* Corresponding author. Tel.: +354 525 4047.
E-mail addresses: eysteinn@hi.is (E.M. Sigurðsson), silvia.valero@cesbio.cnes.fr (S. Valero), benedikt@hi.is (J.A. Benediktsson), jocelyn.chanussot@gipsa-lab.grenoble-inp.fr (J. Chanussot), hugues.talbot@esiee.fr (H. Talbot), einarste@landspitali.is (E. Stefánsson).

http://dx.doi.org/10.1016/j.patrec.2014.03.006
0167-8655/

enough to detect rectilinear and curved structures at the same time. To remedy this limitation, the work presented in [35,33] proposes an infimum of openings using lines as structuring elements oriented in all the possible directions. This method has some inherant problems. For example, for each pixel the structuring element is rotated by discrete steps and the filter is applied after each step. If the steps are too large, there is a great chance of missing a particular vessel since the stucturing element might not align well enough to the direction of the vessel and if the steps are too small the processing time is increased. To address these limitations, directional morphological filters such as path openings [29,31] have been proposed in the last years. These operators have demonstrated their flexibility in order to detect structures that are not strictly linear without depending on their orientation. The first work that proposed the use of these operators in the context of vessel detection was introduced by Valero et al. [32]. In that work, two distinct features are extracted from the fundus retinal images that are later filtered by using path openings. The work presented here is based on [32].

A brief outline of the proposed approach is as follows: First, pre-processing is done as a preliminary step in order to prepare the data for the feature extraction. The consequent feature extraction is based on two vessel properties: (1) vessels appear as dark structures in the image corresponding to the local minima and (2) these connected linear structures can also be considered as the image edges given their contrast and thin appearance. The feature extraction is followed by path opening filtering, which preserves the connected vessels and removes the noise. Hence, in order to take into account the different path opening results obtained by the different features, a data fusion based on fuzzy sets is performed.

The goal here is to introduce a fusion scheme by combining the feature sets taking their respective weights into consideration and produce a final fuzzy set. This set is then used to classify each pixel in the image as belonging to a vessel or not. This method has the distinct advantage of not relying on a single classification or feature extraction method but tries to combine different methods and use the best available information from each of them.

The paper is organized as follows. The pre-processing task removing the noise and enhancing the vessel contrast on color fundus images is explained in Section 2. The feature extraction strategy is explained in Section 3 and the path opening algorithm used to enhance linear structures in the feature images is discussed in Section 4. The proposed data fusion performed on the feature images to construct the final vessel map is presented in Section 5. The evaluation of the proposed method by using real data is addressed in Section 6. In order to assess the quality of the results, they are compared with other vessel detection algorithms in Section 7. Finally, conclusions are drawn in Section 8.

2. Pre-processing

The goal of the pre-processing is to enhance the features of the image to improve the efficiency of the feature extraction algorithms. The importance and the usefulness of the different preprocessing methods that are used here has been extensively studied in [33].

Here, the pre-processing involves histogram equalization and noise reduction. These image transformations are applied consecutively on a gray scale image constructed from the color retinal images where the gray scale conversion of a RGB color fundus image is obtained by preforming a weighted sum of the R, G, and B components with $0.2989R + 0.5870G + 0.1140B$. This is the luminance channel of the YUV color space based on the NTSC standard. The resulting gray scale image is then used to carry out the pre-processing tasks described in Sections 2.1 and 2.2.

2.1. Histogram equalization

Contrast-limited adaptive histogram equalization (CLAHE) [22] is an improved version of the Adaptive histogram equalization (AHE) where the image is divided into contextual regions that are then individually enhanced using histogram equalization. For the AHE model, problems can arise for homogeneous areas which are characterized by a high peak in the histogram. CLAHE introduces *clip limit* that prevents over saturation of the image by accumulating bin values higher that the *clip limit* and distributing the extra amount evenly over all the bins. In this paper the image is divided into 64 regions (8×8 blocks) and the *clip limit* is 0.01.

2.2. Noise reduction

Two filters are applied on the previously obtained grayscale image. Firstly, the non-linear abrupt gray level variations on the image can be considered as an undesired additive noise, which is removed by using a Gaussian filter. In this case, the filtering degree is controlled by the variance of the Gaussian kernel which should correspond to a balanced value. This consideration must be taken into account to avoid that real blood vessels are not lost in the process as explained in [33]. Secondly, to improve the results of the Gaussian filtering, an opening operator is used with a small diamond structuring element to remove the remaining maximum values that are smaller than the structuring element.

3. Feature extraction

Some classical blood vessel patterns can be detected by observing retinal images. The work presented here is focused on two important vessel properties. The first property is related to the fact that vessels appear dark relative to their background. The second property is given by the thin and curvilinear structure of the vessels which is connected to form the well-known vessel tree. Here, both properties are used to define two features images from the previously pre-processed image. Based on the above properties, two features are extracted as described below.

3.1. First feature: local minimum detection

The first feature is extracted using the simple fact that vessels appear darker than their surroundings. To enhance and isolate the vessels, a *black top-hat* [26] operator is used. The Black Top Hat morphological operator is well-known for detecting dark structures smaller than a given structuring element SE. Given an image I and its morphological closing operator $\phi(I)$, the BTH is defined by

$$\mathrm{BTH}(I) = \phi(I) - I \tag{1}$$

where SE of the closing operator is diamond shaped and needs to completely fill vessels in the image. This results in a feature set where most of the background shading has been removed and vessels are clearly visible.

3.2. Second feature: edge detection

The second feature is extracted using an edge detection method called Difference of Gaussian (DoG) [15,5] and is obtained by convolving the image with the difference of a Gaussian kernel with a smaller variance σ_1 and a Gaussian kernel with a larger variance σ_2. The application of this filter on image I is defined by:

$$DoG(I) = G_{\sigma 1} - G_{\sigma 2} \tag{2}$$

where $G_{\sigma 1}$ and $G_{\sigma 2}$ are defined as a convolution of the image using a Gaussian kernel: $G_{\sigma n} = I * \frac{1}{2\pi\sigma_n^2} exp\left(\frac{x^2+y^2}{2\sigma_n^2}\right)$ and $\sigma_2 < \sigma_1$ with negative values then set to zero.

This results in a feature where edges of the vessels are prominent. The downside is that the circular edges or the field of view around the image are also enhanced.

Fig. 1(b) and (c) shows an example of feature images obtained by the procedure described above. As can be observed most of the pixels belonging to the vessel tree have been highlighted in the results. However, it should also be noticed that some background noise has been detected by the feature extraction step as shown in the figures. To remove this noise, the curvilinear shape vessel structure is an important discriminative pattern. Accordingly, the next step in our algorithm is the use of the path opening filters in order to preserve the vessel structures by removing the background noise.

4. Directional filtering

Path openings and closings are algebraic morphological operators used for the analysis of linear and oriented structures [29,31,13,10,36]. In principle, the path opening algorithm lowers the intensity of pixels that are not connected to any path of given minimum length L_{min}. It uses the notion of graph connectivity as a basis for estimating whether a pixel belongs to a path or not. This allows for more flexible curving lines than the more restricted algorithms that use rotating linear structuring elements. In order to be useful, this connectivity should reflect the kind of paths that the application requires. Examples of useful graphs are those that define cones oriented in the principal directions of the grid. Path openings in these graphs are those that retain paths that at each point fit in a 90° angle cone, oriented in a principal direction. Combination by supremum makes it possible to retain paths oriented in all possible directions just using these four adjacencies. Employed in this manner, path openings can be used to retain features that are locally oriented but not necessarily perfectly straight. Path openings can be implemented efficiently both in binary and grey-level cases with a linear time complexity with respect to L_{min} using a decomposition algorithm. Fig. 1(d) and (e) shows the result of the path opening method on the local minimum and the edge detection features.

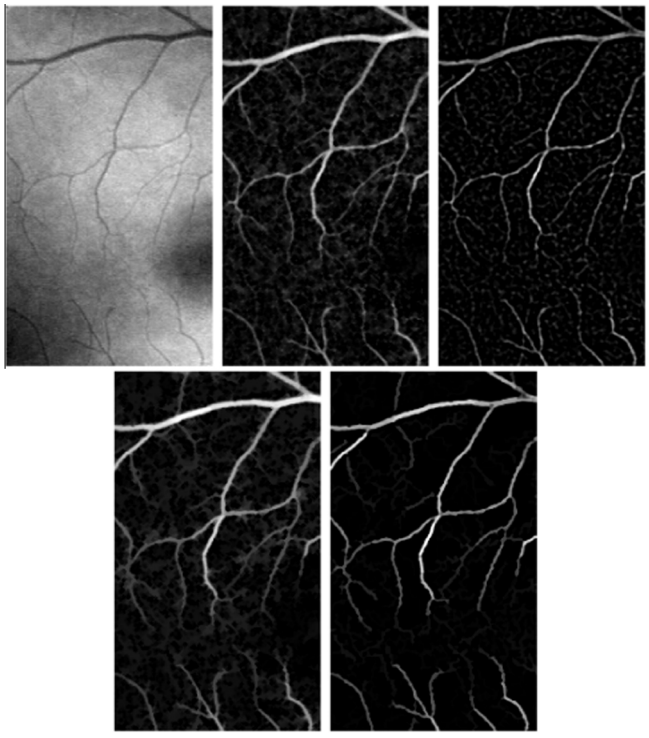

Fig. 1. In the top row (from left to right): (a) original image, (b) local minimum detection and (c) edge detection. Bottom row (from left to right) shows the results of path opening on (d) local minimum detection and (e) edge detection.

5. Information fusion and classification

After completion of the directional filtering, a final vessel map needs to be created where the value of each pixel represents the probability of belonging to a vessel or not. The strategy here is based on considering the information provided by the two path opening results, computed in the previous section, as two independent features I_{f_1} and I_{f_2}.

In order to combine relevant information from different sources, information fusion has demonstrated its advantages in image analysis [1]. In the context of this paper, the fusion scheme aims at classifying the pixels in two classes; vessel v and not vessel nv. That is achieved by merging the I_{f_1} and I_{f_2} information in order to improve the robustness and accuracy in the classification process. The information provided by the two path openings can be considered fuzzy, i.e., both openings are attempting to provide information on the same classification problem and need to be fused. Fuzzy set theory has shown in the past to be attractive for data fusion [3] of classification information. Therefore, the fuzzy approach is selected here.

The fusion process described here is composed of the following two steps: Firstly, the path opening results are interpreted in order to define the two features I_{f_1} and I_{f_2} in terms of fuzzy sets. Secondly, a combination rule [20] based on fuzzy sets is used to aggregate the results provided by the previous step.

5.1. First step: interpreting path opening results as fuzzy sets

The strategy in this step consists of considering each path opening I_{f_j} image as a classification result, where the gray level value reflects the classification reliability. Accordingly, the probability of a pixel belonging to a vessel or not depends on its intensity level. A low intensity (black) implies that the pixel does not belong to a vessel whereas high intensity values (white) imply that the pixel belongs to the vessel tree. The interpretation of the path opening results in terms of fuzzy sets is based on computing membership degree values.

Definition (*Membership degree value*). For a given class n and a pixel p, the membership degree value $\mu_j^n(p)$ represents the degree of truth that p could belong to n according to classifier j.

Definition (*Fuzzy set*). In a m-class classification, a fuzzy set $\pi_j(p)$ is the set of m membership degree values assigned to one pixel p by one classifier j.

The membership degree value computed at each pixel p describes whether p belongs to the vessel $\mu_j^v(p)$ or non vessel class $\mu_j^{nv}(p)$. Given our two-class classification application, the fuzzy set computed for each pixel $\pi_j(p)$ assigned by each I_{f_j} is defined as the set of two membership degree values:

$$\pi_j(p) = \left\{\mu_j^v(p), \mu_j^{nv}(p)\right\} \quad j = [1,2] \tag{3}$$

As mentioned above, the gray level intensity of p at path opening results I_{f_1} and I_{f_2} is used to obtain the values of the membership functions $\mu_j^v(p)$ and $\mu_j^{nv}(p)$. Using this consideration and assuming that the feature images have pixel values between 0 and 1, the membership functions $\mu_j^v(p)$ and $\mu_j^{nv}(p)$ are defined as:

$$\mu_j^{v}(p) = K_1 - Feature_j(p)$$
$$\mu_j^{nv}(p) = K_2 - (1 - Feature_j(p)) \quad (4)$$

where K_1 and K_2 are constants that make the two-class classification algorithm less restrictive with typical values around 0.1 and 1.1, respectively. Here, a less restrictive classification means that not only pixels with values around 1 can be interpreted as vessels.

5.2. Second step: combination rules

The two different fuzzy sets resulting from the two path opening results, need to be combined into a single fuzzy set $\pi(p) = \{\mu^v(p), \mu^{nv}(p)\}$. To address that, it is important to measure how *fuzzy* a fuzzy set is, and, thus, estimate the ambiguity of the set. Several ways are available to the measure fuzziness [20,3] degree of $pi_1(p)$ and $pi_2(p)$. One such approach that has previously shown a good performance [3] is based on the multiplicative class.

The multiplicative class is defined as:

$$H_*(\mu_F) = K\sum_{i=1}^{n} g(\mu_F(x_i)), \quad K \in R^+ \quad (5)$$

where $g(\mu_F)$ is defined as:

$$g(t) = \tilde{g}(t) - \min_{0\leqslant t\leqslant 1}\tilde{g}(t)$$
$$\tilde{g}(t) = h(t)h(1-t) \quad (6)$$

and h is a concave increasing function on [0, 1].

Definition (*Fuzziness degree*). The fuzziness degree is a measure of uncertainty to estimate the ambiguity of a fuzzy set.

By modifying the function $h\,(t)$ it is possible to change the definition of the fuzziness measures. Here $h(t)$ is selected as $h(t) = t^{\alpha}$ where $0 \leqslant \alpha \leqslant 1$. This selected $h(t)$ function satisfies the required conditions for the multiplicative class and is a concave increasing function on $[0, 1]$. Using this $h(t)$, the measure of fuzziness [20,3] is defined as:

$$H_{\alpha QE}(\pi(p)) = \frac{1}{n2^{-2\alpha}}\sum_{i=1}^{n}\mu_F(x_i)^{\alpha}(1-\mu_F(x_i))^{\alpha} \quad (7)$$

where n is the number of features and α is the sensitivity of the degree of fuzziness. When α is close to 0, all fuzzy sets are measured with the same degree of fuzziness while α close to 1 makes the degree of fuzziness highly sensitive and quickly decreasing when the fuzzy set differs from $\mu_F = 0.5$. To get balanced results, $\alpha = 0.5$ is a reasonable choice [20].

By using the fuzziness degree to estimate the quality of fuzzy sets, it is possible to put more emphasis on the quality of information. This is done by deriving relative weights for each fuzzy set:

$$w_i = \frac{\sum_{k=0}^{m} H_{\alpha QE}(\pi_k)}{(m-1)\sum_{k=0}^{m} H_{\alpha QE}(\pi_k)} \quad (8)$$

where $\sum_{i=0}^{m} w_i = 1, \alpha = 0.5, m$ the number of fuzzy sets and w_i the relative weight of fuzzy set i.

This allows for a final fuzzy set using the weights:

$$\mu^{v}(p) = max(w_i\mu_i^{v}(p)) \quad i = [1, n]$$
$$\mu^{nv}(p) = max(w_i\mu_i^{nv}(p)) \quad i = [1, n] \quad (9)$$

The defuzzification process is then simply:

$$\mu^{v}(p) > \mu^{nv}(p) \quad \text{pixel } p \text{ is a vessel}$$
$$\mu^{v}(p) \leqslant \mu^{nv}(p) \quad \text{pixel } p \text{ is a non-vessel} \quad (10)$$

6. Experimental results

6.1. Presentation of the data used

The DRIVE [27] data set is used here in order to evaluate the methodology presented in the previous sections. This data set is a collection of 40 retinal images randomly selected from a diabetic retinopathy screening program in the Netherlands. For each image, a mask image is provided that delineates the FOV. The images are divided into two categories containing 20 images each, one used for training and another for testing. For the test set, two manual segmentations have been made, one of which can be considered the gold standard. For the training set, a single manual segmentation has been made. Each image has three bands and a dimension of 565×584 pixels. The mask and the manually segmented images are binary images of the same dimensions.

The image shown in Fig. 2(a) is used in the following in order to show the different results obtained at the various stages of the proposed methodology. This particular image was chosen for a few reasons. It is a fairly typical fundus image with the optic disk clearly visible in the right part of the image and the darker macula in the center. The background shading is fairly uneven with higher intensity areas around the center. The image contains possible pathology, evident by the high intensity pixels around the vessels in the lower right part. The goal is to isolate the major arteries with as little interference due to the macula and optic disk as possible and to get acceptable accuracy when compared to a manually segmented image.

6.2. Example

The original image is first preprocessed. After histogram equalization, the image is filtered with a small Gaussian kernel of size 3 pixels with a standard deviation of 0.6. This softens out the noisy pixels but still preserves enough details. To suppress the noise even further, an opening operator is used with a diamond structuring element of 1 pixel in size. The result can be seen in Fig. 2(b).

The first feature is found by using local minimum detection. To isolate the vessels, the BTH(f) operator (Eq. (1)) is used on the image. To fill the vessels completely, a closing operator was used with diamond structuring element, 8 pixels in size.

Looking at Fig. 3(a), it can be seen that the intensity of the vessels has been enhanced. However, some significant noise is still present in the background. By using the path opening operator, it is possible to preserve line structures while eliminating some of the noise. The L_{min} must be chosen as the minimal length vessel that should be preserved in the images. For this application, a threshold value of $L_{min} = 34$ is considered to be adequate. The obtained results are shown in Fig. 3(b).

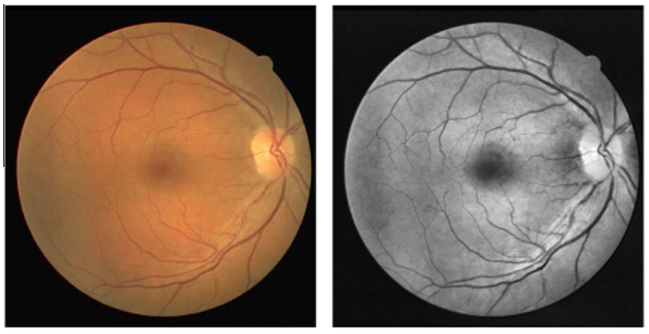

Fig. 2. Image number 28 from the DRIVE data set (a) in its original form and (b) after preprocessing.

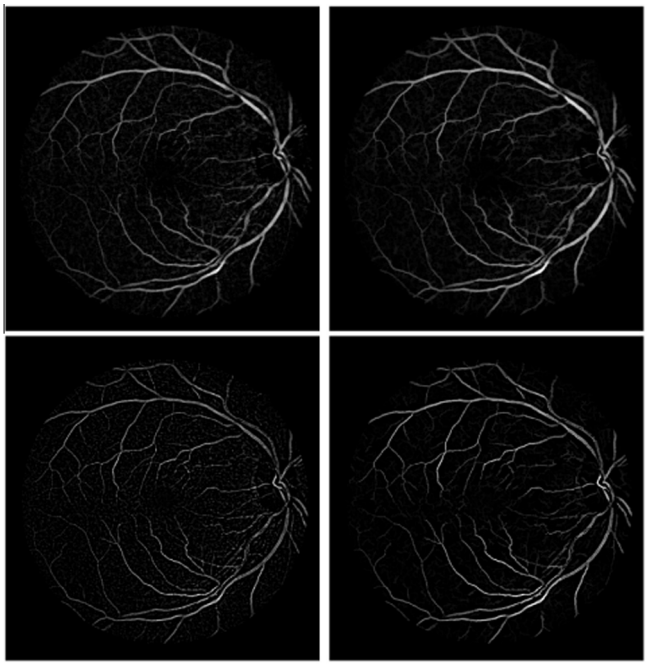

Fig. 3. Top row (from left to right) shows the 1st feature (a) after BTH(f) operator and (b) after path opening. Bottom row (from left to right) shows the 2nd feature (c) after DoG operator and (d) after path opening.

The second feature is computed using edge detection. The quality of the edge detection depends on the σ_1 and σ_2 values as well as the window size of the two Gaussian filters. The choice of the sigma values changes the amount of detail in the resulting image. Therefore, σ is an important parameter. Large values of σ allow for detection of smaller vessels but also introduce incorrectly detected vessels. For this reason, the values are set as $\sigma_1 = 1.75$ and $\sigma_2 = 0.8$. The value of window depends on the greatest vessel width in the image, which in this case is estimated to be 15 pixels.

After applying the DoG operator (Fig. 3(c)), noise is significant in the image. Some of the noise is filtered out using the path opening operator[1] (Fig. 3(d)) with the same threshold as before, $L_{min} = 34$.

Once the two complementary feature sets have been defined, the data fusion scheme is used to construct a fuzzy set to ascertain if a pixel belongs to a vessel or not. Firstly, the feature set is fuzzified to create a membership function (Eq. (4)). The values used for K are $K_1 = 1.1$ and $K_2 = 0.1838$. Secondly, the fuzziness degree, $H_{\alpha QE}(\pi(p))$ (Eq. (7)) is estimated for each feature and the resulting fuzzy set is weighted accordingly (Eq. (8)). Experiments show that in practice the second feature is slightly more important and usually gets marginally greater weight. Thirdly, a new fuzzy set is created using the combination rules (Eq. (9)). Now it is straight forward to do the pixel classification using this new fuzzy set. The final vessel map (Fig. 4(a)) shows that all the major vessels are clearly visible and identified. However, the finer vessels are less likely to be detected. The final result is then compared to the manual segmented image in Fig. 4(b). All pixels that are incorrectly classified as vessels are marked as false positive and pixels incorrectly classified as non-vessels are marked as false negative. Correctly classified pixels are true positives. Fig. 4 shows the vessel map with incorrectly classified pixels superimposed on Fig. 4(b).

Next, a method is needed to evaluate the accuracy of vessel classification. The image is given a value in accordance with how closely it matches the manually segmented image. The accuracy

[1] The source code for the path openings is available online at https://github.com/path-openings/morphological_path_operators.

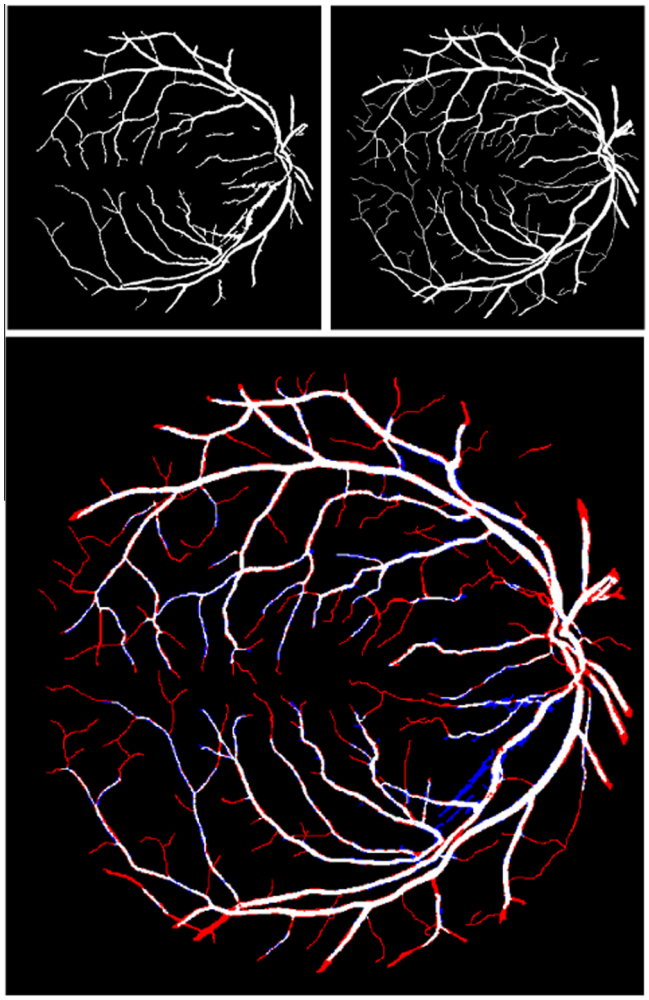

Fig. 4. Pixel classification result using the (a) proposed approach on the top-left, (b) actual manually segmented vessel map from DRIVE data set on the top-right. Bottom image is a (c) vessel map where red denotes false-negatives, blue denotes false-positives and white denotes true-positives. (For interpretation of the references to color in this figure legend, the reader is referred to the web version of this article.)

of a classified image is computed as the total number of correctly classified pixels as a fraction of total pixels within the FoV.

$$Accuracy = \frac{tp + tn}{tp + tn + fp + fn} \tag{11}$$

where tp, tn, fp and fn is the number of true-positive, true-negative, false-positive and false-negative pixels, respectively. One of the benefits of this method is that it is possible to control to some extent whether the classification should emphasize to minimize false-negative or false-positive error margins by shifting the fuzzyfication constants K_1 and K_2. Fig. 5 shows this effect by sliding K_2. In this example, however, the combined error ($fn + fp$) was minimized by using a cost function (Eq. (11)) by using $K_1 = 1.1$ and adjusting K_2. However, sometimes it can be desirable to minimize one at the cost of the other. The cost function is minimized for K_2 by selecting $K_1 = 1.1$ so the overall error is minimized.

6.3. Quantitative evaluation

Unfortunately, manually segmented images do rarely exist in real life situations and, thus, are not available for reference to minimize the cost function. Therefore, it is important to generalize the

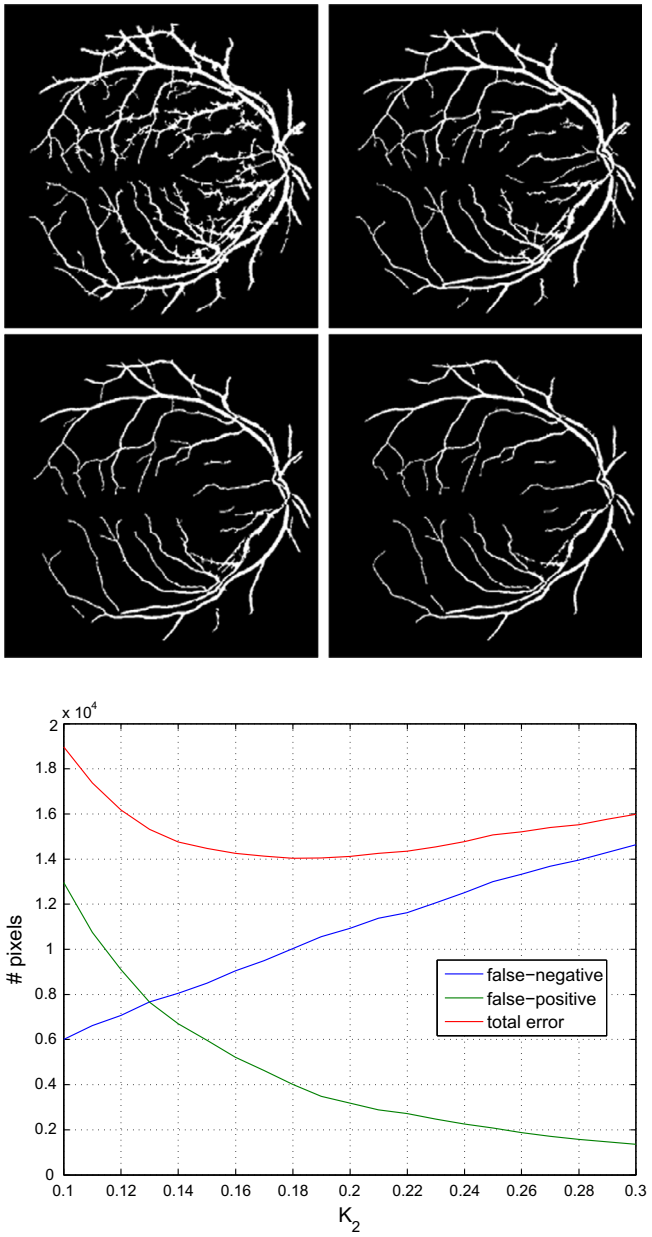

Fig. 5. The sensitivity can be altered by changing K_2. From top-left to right then back to 2nd row left: (a) $K_2 = 0.1$, (b) $K_2 = 0.1667$, (c) $K_2 = 0.2333$, (d) $K_2 = 0.3$. Bottom graph (e) graphically shows how the error can be minimized by changing K_2. This graph shows that the total error is minimized around $K_2 = 0.18$.

fuzzy constants. As mentioned previously, the DRIVE data set is divided into training and test sets. The most obvious solution is to find the optimal fuzzy constants K_2 for the training set and use those results for the test set. Table 1 shows the optimal fuzzy constant K_2 and the overall accuracy for each image in the training set. Kappa is a measure of agreement between the image and the gold standard [14]. By taking the median of K_2, a rough estimate of the most common fuzzy constant is found as $K_2 = 0.2051$. This constant is then used to analyze the test set. After estimating the vessel map, the results are compared to manually segmented images where Accuracy_1 is considered the gold standard. These results are given in Table 2.

To help visualizing the vessel classification, two images are chosen and plotted. The image shown in Fig. 6(a) corresponding to the third image in the DRIVE data set is selected first since the classifier seems to struggle with it, given its relatively low accuracy score for

Table 1
Optimal fuzzy constants K_2 and accuracy for the training set.

Image #	Optimal K_2	Kappa	Accuracy
21	0.2102	0.7698	0.9581
22	0.1731	0.7244	0.9432
23	0.5021	0.5863	0.9436
24	0.1527	0.7576	0.9376
25	0.1307	0.6869	0.9329
26	0.2896	0.6922	0.9409
27	0.1530	0.7282	0.9452
28	0.1838	0.7244	0.9384
29	0.1777	0.7080	0.9436
30	0.1975	0.7042	0.9460
31	0.2675	0.6567	0.9533
32	0.1956	0.7341	0.9484
33	0.2522	0.7434	0.9512
34	0.3014	0.5544	0.9097
35	0.2348	0.7529	0.9504
36	0.1844	0.7107	0.9280
37	0.2182	0.7171	0.9436
38	0.2114	0.7321	0.9449
39	0.2000	0.7420	0.9459
40	0.3001	0.7419	0.9526
Median	0.2051	0.7244	0.9443
Mean	0.2268	0.7084	0.9429

Table 2
Accuracy for the test set using $K_2 = 0.2051$.

Image #	Accuracy_1	A_z	Accuracy_2
1	0.9465	0.9540	0.9507
2	0.9488	0.9533	0.9558
3	0.9315	0.9217	0.9430
4	0.9452	0.9276	0.9533
5	0.9451	0.9294	0.9624
6	0.9397	0.9250	0.9474
7	0.9379	0.9197	0.9588
8	0.9383	0.9199	0.9526
9	0.9482	0.9268	0.9519
10	0.9458	0.9330	0.9585
11	0.9436	0.9242	0.9559
12	0.9472	0.9362	0.9557
13	0.9364	0.9238	0.9366
14	0.9499	0.9500	0.9568
15	0.9523	0.9446	0.9500
16	0.9481	0.9513	0.9575
17	0.9399	0.9317	0.9486
18	0.9516	0.9534	0.9517
19	0.9596	0.9638	0.9483
20	0.9536	0.9563	0.9433
Median	0.9461	0.9323	0.9523
Mean	0.9455	0.9373	0.9519

$\text{Accuracy}_1 = 0.9315$ and $\text{Accuracy}_2 = 0.9430$ in Table 2. By examining the classification results it is easy to see that the pathology, manifesting itself as bright spots in the lower part of the image, is confusing the classifier. This is mostly because the pre-processing step uses abrupt changes in pixels intensity values to identify possible vessels. The relative lower intensity pixels in-between closely packed and high intensity spots can be misinterpreted as the local intensity minimum of a vessel signature. Therefore, it is not directly the spots that confuse the classifier but rather their proximity to each other which, in turn, creates local minimas in-between them. One possible solution to this would be to identify this pattern in the preprocessing steps and then use a morpological closing operator to fill in the gaps, since it is unlikely that they contain actual vessels. The second image chosen corresponds to the 19th image in the DRIVE data set and is shown in Fig. 6(b). The results from the vessel extraction in Table 2 shows a relatively high Accuracy_1 score but an Accuracy_2 score that is below average. All the major vessels are accounted for in the classification, while

Fig. 6. Original images (left) and its corresponding vessel map (right). Top row (a) shows the worst case classification while the bottom row (b) shows the best case classification.

some of the smaller ones are partially missing. One of the reason for the relatively high accuracy that was obtained could be the lack of any obvious pathology.

7. Comparison with other methods

There are few ways of comparing this method to existing methods. The accuracy value is determined by how many correctly classified vessel pixels and non-vessel pixels are as a fraction of total pixels inside the FoV. First the optimal value for the fuzzy constant K_2 is found using the training set. This should theoretically give the maximum accuracy for the test set as well. Then, to determine the maximum average accuracy (MAA), the average accuracy value for all the test set taken using the computed value for K_2. If the method in question is based on a soft classification, meaning that the intensity of the pixel determines its probability of belonging to a vessel or not, then a sensitivity/specificity chart can be made by thresholding the classifier. A ROC curve is computed by using a range of values for K_2 which plots the true-negative fraction against false-positive fraction (see Fig. 7). The area under the ROC curve (A_Z) indicates the discriminatory ability of the vessel tracking method, with a value of 1 being perfect classification and 0.5 being random classification.

Table 3 compares a few vessel tracking methods to the method proposed in this paper. The second column contains the maximum average accuracies with standard deviation in parentheses and A_z measures the area under the RoC curve [18]. By comparing them with the mean Accuracy_1 and A_z from Table 2 it is possible to see that the proposed method outperforms the older well established methods. State-of-the-art methods such as [17] give similar results in terms of accuracy but since A_z is not available an explicit comparison is difficult. The most recent paper of [23] outperforms all other methods significantly.

Gegúndez-Arias et al. [6] propose a novel method to compare vessel segmentation methods. A quality evaluation function (QEF) is developed that takes three parameters as input describing the segmented vessel tree when compared to the gold standard;

Table 3
Comparison for different methods. Results for other methods from [18,23,17].

	Max. avg. Accuracy (Std.)	A_z
2nd Observer	0.9473 (0.0048)	–
Ricci and Perfetti [23]	0.9595	0.9633
Soares et al. [25]	0.9466	0.9614
Mendonca and Campilho [17]	0.9463 (0.0064)	–
Method proposed in this paper	0.9455 (0.0067)	0.9373
Staal et al. [28]	0.9441	0.9520
Zana and Klein [35]	0.9377 (0.0077)	0.8984
Jiang and Mojon [12]	0.9212 (0.0076)	0.9114
Martínez-Pérez et al. [16]	0.9181 (0.0240)	–
Chaudhuri et al. [2]	0.8773 (0.0232)	0.7878
All background	0.8727 (0.0123)	–

connectivity (C), area (A) and length (L). Each parameter has a range of [0,1] where 1 is a perfect score. The final function is product of these three parameters:

$$f(C,A,L) = C * A * L \tag{12}$$

The paper gives results for various different vessel segmentation algorithms presented in the literature where image number 2 of the test set used in this paper (from DRIVE database) is analyzed. The mean score for all the methods evaluated in [6] is $\overline{f(C,A,L)} = 0.6674$. If the same analysis is done on image 2 using the method proposed in this paper, the QEF score is found to be $f(0.9891, 0.8957, 0.7939) = 0.7033$ while the mean score for proposed method on the whole training set (all 20 images in the DRIVE database) is $\overline{f(C,A,L)} = 0.6274$.

8. Discussion and conclusion

In this paper an automatic vessel extraction method based on path openings for fundus images has been proposed. The proposed technique assumes that the vessels are connected linear structures. The nature of the path opening filter makes it an ideal candidate to enhance vessels since they are linear but not necessarily straight structures, which is often a problem when classical morphological operators are concerned. The method is completely unsupervised and does not need any specific training. While most of the parameters are set during the methodology steps it is still quite extensible. Experimental results in the paper show the method to give good results. Furthermore, the method demonstrates an ability to isolate major vessels and many of the minor vessels with a similar or better accuracy than many other vessel segmentation methods without incurring a high computational cost.

There are some inherent problems when deciding the accuracy of a classified image. Since the reference images are manually classified, there is always some degree of human error, as is evident by the fact that even the two manually segmented images do not match each other completely. However, that is perfectly normal, since the observers are asked to mark pixels that they are 70% sure are vessels. In addition, each pixel receives the same amount of weight and no consideration is given to the seriousness of the error. For example, a pixel that is misclassified close to a vessel could be considered a less severe error then a disconnected pixel that is misclassified.

By using the training set to find a median value for the fuzzification constant K_2, the classification becomes simple. This method has been shown to perform sufficiently but is not guaranteed to give an optimal performance in terms of accuracies since it is only based on relatively a small training set. The weights in the data fusion scheme alleviate this problem since less weight is put on unreliable data but that is not a perfect solution. One idea for future work would be to make the fuzzification constant adaptable using some data characteristics on per image basis. In the paper,

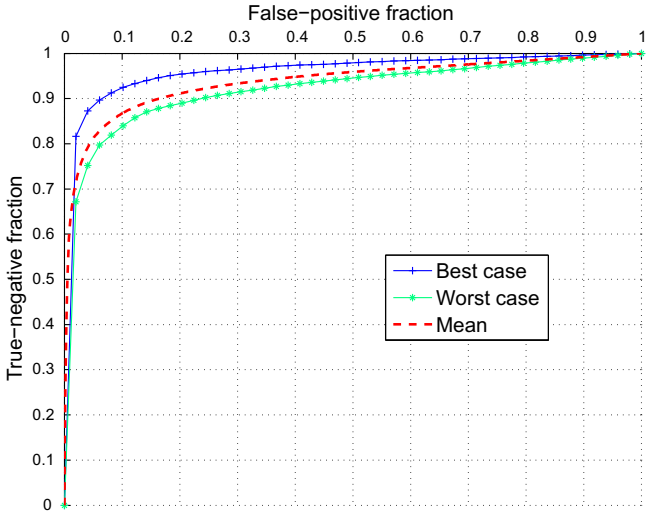

Fig. 7. ROC curves for the worst (Fig. 6(a)) and the best (Fig. 6(b)) cases. The mean curve for the whole test data set is plotted for reference.

two distinct features were used for the data fusion scheme. Perhaps it is possible to extract more features with various other methods to get even better results. That could potentially improve the results where images vary (due to pathology, etc.) since some methods would provide more or less reliable data in certain situations, more weight would then be put on the more crisp fuzzy sets and the data would therefore be sorted for reliability.

The mean processing time for classification is 0.57 s for each image. If the whole training set is used then the training time to find the optimal K2 is 33.76 s. The computer used was an Intel Core i5-3570 CPU running at 3.40 GHz with 8 GB of RAM although memory consumption is much lower. Therefore classification could be considered to be performed in near real-time.

Acknowledgments

This research was supported in part by the Icelandic Research Fund and the Research Fund of the University of Iceland.

References

[1] I. Bloch, Fusion d'informations en Traitement du Signal et des Images, Hermes Science Publications, 2003.
[2] S. Chaudhuri, S. Chatterjee, N. Katz, M. Nelson, M. Goldbaum, Detection of blood vessels in retinal images using two-dimensional matched filters, IEEE Trans. Med. Imaging 8 (1989) 263–269.
[3] M. Fauvel, J. Chanussot, J. Benediktsson, Decision fusion for the classification of urban remote sensing images, IEEE Trans. Geosci. Remote Sens. 44 (2006) 2828–2838.
[4] L. Gang, O. Chutatape, S.M. Krishnan, Detection and measurement of retinal vessels in fundus images using amplitude modified second-order gaussian filter, IEEE Trans. Biomed. Eng. 49 (2002) 168–172.
[5] X.W. Gao, A. Bharath, A. Stanton, A. Hughes, N. Chapman, S. Thom, Quantification and characterisation of arteries in retinal images, Comput. Meth. Programs Biomed. 63 (2000) 133–146.
[6] M.E. Gegúndez-Arias, A. Aquino, J.M. Bravo, D. Marin, A function for quality evaluation of retinal vessel segmentations, IEEE Trans. Med. Imaging 31 (2012) 231–239.
[7] J. Hajer, H. Kamel, E. Noureddine, Blood vessels segmentation in retina image using mathematical morphology and the STFT analysis, in: Information and Communication Technologies, 2006. ICTTA'06, second ed., IEEE, 2006, pp. 1130–1134.
[8] S. Hardarson, E. Stefansson, Oxygen saturation in central retinal vein occlusion, Am. J. Ophthalmol. 150 (2010) 871–875.
[9] S. Hardarson, E. Stefánsson, Retinal oxygen saturation is altered in diabetic retinopathy, Br. J. Ophthalmol. 96 (2012) 560–563.
[10] H. Heijmans, M. Buckley, H. Talbot, Path openings and closings, J. Math. Imaging Vision 22 (2005) 107–119.
[11] A. Hoover, V. Kouznetsova, M. Goldbaum, Locating blood vessels in retinal images by piecewise threshold probing of a matched filter response, IEEE Trans. Med. Imaging 19 (2000) 203–210.
[12] X. Jiang, D. Mojon, Adaptive local thresholding by verification-based multithreshold probing with application to vessel detection in retinal images, IEEE Trans. Pattern Anal. Mach. Intell. 25 (2003) 131–137.
[13] S. Klemenjak, B. Waske, S. Valero, J. Chanussot, Automatic detection of rivers in high-resolution SAR data, IEEE J. Sel. Top. Appl. Earth Obs. Remote Sens. 5 (2012) 1364–1372.
[14] J.R. Landis, G.G. Koch, The measurement of observer agreement for categorical data, Biometrics 33 (1977) 159–174.
[15] J. Lowell, A. Hunter, D. Steel, A. Basu, R. Ryder, R.L. Kennedy, Measurement of retinal vessel widths from fundus images based on 2-d modeling, IEEE Trans. Med. Imaging 23 (2004) 1196–1204.
[16] M.E. Martínez-Pérez, A.D. Hughes, A.V. Stanton, S.A. Thom, A.A. Bharath, K.H. Parker, Retinal blood vessel segmentation by means of scale-space analysis and region growing, in: Medical Image Computing and Computer-Assisted Intervention–MICCAI99, Springer, 1999, pp. 90–97.
[17] A.M. Mendonca, A. Campilho, Segmentation of retinal blood vessels by combining the detection of centerlines and morphological reconstruction, IEEE Trans. Med. Imaging 25 (2006) 1200–1213.
[18] M. Niemeijer, J. Staal, B. van Ginneken, M. Loog, M. Abramoff, Comparative study of retinal vessel segmentation methods on a new publicly available database, in: SPIE Medical Imaging, Proc. SPIE, 2004, pp. 648–656.
[19] O. Olafsdottir, S. Hardarson, M. Gottfredsdottir, A. Harris, E. Stefánsson, Retinal oximetry in primary open-angle glaucoma, Invest. Ophthalmol. Visual Sci. 52 (2011) 6409–6413.
[20] N. Pal, J. Bezdek, Measuring fuzzy uncertainty, IEEE Trans. Fuzzy Syst. 2 (1994) 107–118.
[21] D. Paulus, S. Chastel, T. Feldmann, Vessel segmentation in retinal images, in: Proc. of SPIE, 2005, p. 697.
[22] A.M. Reza, Realization of the contrast limited adaptive histogram equalization (CLAHE) for real-time image enhancement, J. VLSI Signal Process. Syst Signal Image Video Technol. 38 (2004) 35–44.
[23] E. Ricci, R. Perfetti, Retinal blood vessel segmentation using line operators and support vector classification, IEEE Trans. Med. Imaging 26 (2007) 1357–1365.
[24] C. Sinthanayothin, J.F. Boyce, H.L. Cook, T.H. Williamson, Automated localisation of the optic disc, fovea, and retinal blood vessels from digital colour fundus images, Br. J. Ophthalmol. 83 (1999) 902–910.
[25] J.V. Soares, J.J. Leandro, R.M. Cesar, H.F. Jelinek, M.J. Cree, Retinal vessel segmentation using the 2-d Gabor wavelet and supervised classification, IEEE Trans. Med. Imaging 25 (2006) 1214–1222.
[26] P. Soille, Morphological Imgae Analysis: Principles and Applications, Springer-Verlag New York, Inc., 2003.
[27] J. Staal, M. Abràmoff, M. Niemeijer, M. Viergever, B. van Ginneken, Ridge-based vessel segmentation in color images of the retina, IEEE Trans. Med. Imaging 23 (2004) 501–509.
[28] J. Staal, M.D. Abràmoff, M. Niemeijer, M.A. Viergever, B. van Ginneken, Ridge-based vessel segmentation in color images of the retina, IEEE Trans. Med. Imaging 23 (2004) 501–509.
[29] H. Talbot, B. Appleton, Efficient complete and incomplete path openings and closings, Image Vision Comput. 25 (2007) 416–425.
[30] S. Traustason, A. Jensen, H. Arvidsson, I. Munch, L. Sndergaard, M. Larsen, Retinal oxygen saturation in patients with systemic hypoxemia, Invest. Ophthalmol. Visual Sci. 52 (2011) 5064–5067.
[31] S. Valero, J. Chanussot, J. Benediktsson, H. Talbot, B. Waske, Advanced directional mathematical morphology for the detection of the road network in very high resolution remote sensing images, Pattern Recognit. Lett. 31 (2010) 1120–1127.
[32] S. Valero, J. Chanussot, J.A. Benediktsson, H. Talbot et al., Détection automatique du réseau vasculaire rétinien basée sur la morphologie directionnelle et la fusion de décision, in: XIIe Colloque GRETSI, 2009.
[33] T. Walter, J.C. Klein, Segmentation of color fundus images of the human retina: detection of the optic disc and the vascular tree using morphological techniques, in: Medical Data Analysis, Springer, 2001, pp. 282–287.
[34] Y. Yang, S. Huang, N. Rao, An automatic hybrid method for retinal blood vessel extraction, Int. J. Appl. Math. Comput. Sci. 18 (2008) 399–407.
[35] F. Zana, J.C. Klein, Segmentation of vessel-like patterns using mathematical morphology and curvature evaluation, IEEE Trans. Image Process. 10 (2001) 1010–1019.
[36] F. Cokelaer, H. Talbot, J. Chanussot, Efficient robust d-dimensional path operators, IEEE J Selected Top. Signal. Proc. 6 (2012) 830–839.